European Journal of Mechanics / B Fluids 105 (2024) 338–345

Contents lists available at ScienceDirect

European Journal of Mechanics / B Fluids

journal homepage: www.elsevier.com/locate/ejmflu

Influence of passive deformation in the lift coefficient of a NACA0012 wing model

E. Duran [a,*], M. Lorite-Díez [a,b,c], N. Konovalov-Shishov [a], P. Gutierrez-Castillo [a], C. del Pino [a]

[a] Department of Mechanical, Thermal and Fluids Engineering, Universidad de Málaga, Málaga, Spain
[b] Andalusian Institute for Earth System Research, University of Granada, Granada, Spain
[c] Departamento de Mecánica de Estructuras e Ingeniería Hidráulica, Universidad de Granada, Spain

ARTICLE INFO

Keywords:
Lift coefficient
Passive deformation
NACA0012
Aspect ratio

ABSTRACT

The extensive use of lightweight materials in aerial vehicle wings involves structural flexibility phenomena that generate non-negligible deformation effects. This influence is not restricted to big aircraft but also plays a role in smaller aeroplanes and Unmanned Aerial Vehicles (UAVs). Here, we conduct wind tunnel experiments to analyze the effect of passive deformation on the wing model lift slopes. To isolate the deformation effect, we compare rigid wings with a NACA0012 airfoil imposing a prescribed spanwise deformation. We study three levels of deformation: non-deformed, around 2% and 4.5% of tip deflection. Also, we consider the effect of the wing length by using three different semi-aspect ratios (1, 2, and 4), so a total of nine rigid wing models have been analyzed for a range of Reynolds number from 80×10^3 to 160×10^3. Deformed wing models show an increase in lift coefficient compared to non-deformed wing cases. Both deformation levels exhibit a qualitatively similar lift increment. A correlation to predict lift coefficient slope in a flat plate is adapted for a NACA0012 airfoil and validated using our experimental results and literature data. The adjusted correlation can quantify the deformation effect on the lift slope, which is comparable to using a slightly longer wing model.

1. Introduction

Researchers have traditionally considered air vehicle wings as rigid parts throughout most experimental studies to determine aerodynamic characteristics. However, nowadays, the extensive use of lightweight materials entails some structural flexibility. The aerodynamic forces acting on the newly developed slender large aspect ratio wings could provoke significant deformations. In the case of aircraft, deformations of more than 10% of half wingspan have been observed even at cruise flight [1]. This effect appears to be not restricted to aircraft but is also relevant in smaller military aeroplanes, low-speed near space aircraft or Unmanned Aerial Vehicles (UAVs) [2,3]. Therefore, studying the aerodynamic impact of possible wing deformations is crucial in many aerial applications. Also, the deformation effects are relevant at different flow regimes over a wide range of Reynolds numbers.

Given the importance of the eventual flexibility of real wings and its effect on the flight performance of air vehicles, the scientific and industrial communities have devoted several studies to this topic in recent years. Firstly, at a large Reynolds number, Afonso et al. [4] conducted a thorough review of the recent advances in the role of flexibility for high aspect ratio wings. Moreover, Zhong et al. [5] analyzed the effect of static deformation at high Reynolds number and aspect ratios on a whole aircraft model using experimental and numerical approaches. Additionally, several works have studied the dynamic response and stability of the associated structure under specific flow regimes for long aeroelastic wings [6–8].

On the other hand, the scientific community is also interested in the effect of the deformation on intermediate or low Reynolds number regimes closer to the range studied here. Several authors [9–11] showed how the aerodynamic coefficients (including the slope of the lift coefficient) of flexible micro air vehicle (MAV) wings of low aspect ratio at low Reynolds number can either grow or decrease depending on the geometry of the wing and the settings of flexible parts. Furthermore, the aerodynamic performance of flexible wings under flapping conditions (typical of bio-inspired UAVs) and the influence of their aspect ratio have also attracted attention lately [12–16].

One of the main factors characterizing the aerodynamic performance of wings is the lift coefficient, C_L, and its slope versus the angle of attack, $C_{L\alpha}$. This latter parameter has been studied in the literature for different wing shapes due to its connection to flight

* Corresponding author.
E-mail address: eduran@uma.es (E. Duran).

https://doi.org/10.1016/j.euromechflu.2024.02.007
Received 10 December 2023; Received in revised form 15 January 2024; Accepted 15 February 2024
Available online 17 February 2024

requirements and their influence on induced drag computation [17–19]. A recent study has provided correlations of the $C_{L\alpha}$ of a straight flat plate for any aspect ratio (between 1 and 8) and Reynolds number (ranging from 40 to 200×10^3) [20]. However, the estimations of $C_{L\alpha}$ for NACA0012 wing models become more complicated due to the appearance of non-linear effects as the production of negative lift at positive and small angles of attack near zero at moderate Reynolds number [21]. In the case of a NACA0012 wing model, the onset of negative lift or a dead band [3] appears to be primarily related to both temporal and spatial two-dimensional periodic patterns, and to the upstream flow pre-alignment of the airfoil [21]. Tank et al. [22] also presented a study summarizing the reasons for the measurement discrepancies in the literature for a NACA0012 wing model at moderate Reynolds numbers. A correlation was proposed for a slightly higher Reynolds number to estimate the lift coefficient slope for a semi-aspect ratio equal to 2 and different Reynolds numbers containing results obtained from several authors [23]. Some authors compared flat plates and NACA0012 wing models, finding similar lift coefficients at angles of attack equal to 6.5° [24]. In addition to the complexity of analyzing C_L and $C_{L\alpha}$ for different wing shapes, wing flexibility and its associated deformations mentioned above result in a non-negligible change in the lift coefficient [5].

Despite the number of works analyzing wing deformation and its effect on aerodynamics, the impact of the deformation is coupled with other mechanical problems such as aeroelastic phenomena, unsteady dynamics, or complex wing structures, making it challenging to identify just the effect of wing deformation compared to a non-deformed case. With this work, we aim to isolate the aerodynamic influence of passive wing deformations from other degrees of freedom, such as flexibility. Specifically, we perform wind tunnel experiments with rigid wing models, with and without an imposed deformation, to extract the effect of deformation on the lift coefficient. In particular, we compare the non-deformed case with two deformed geometries extracted from experimental measurements of flexible wings [25]. We test the effect of the deformation on the force coefficients varying the level of wing deflection, the aspect ratio and the Reynolds number. These results could be used to predict essential aerodynamic parameters for different applications and could help to design wing models of UAVs at low Reynolds numbers.

The structure of the paper is the following: in Section 2, we present the details of the experimental setup, including the geometry of the deformed wings. We also describe the different configurations tested regarding aspect ratio, Reynolds number and the level of deformation. We introduce the results of our study by validating our experimental data in Section 3.1. In Section 3.2, we analyze the effect of the deformation in the C_L coefficient for different aspect ratios and Reynolds numbers. In Section 3.3, we discuss an expression to approximate $C_{L\alpha}$ for NACA0012 wing models, comparing it with other results in the literature and evaluating its accuracy for deformed wings. Then, we used the $C_{L\alpha}$ expression in Section 3.4 to relate the deformation effect with the wing aspect ratio. Finally, in Section 4, we present the conclusions, summarizing the main results and the possible contribution from the present study.

2. Outline of the experiment

Wing model forces were obtained under different conditions using a wind tunnel located at the aero-hydrodynamic lab at the University of Málaga. The wind tunnel has a 1 × 1 m^2 cross-section with low turbulence (of the order of 0.8%, see more details in [20]). Each wing model has a c = 100 mm chord, with a length, l, from 100 to 400 mm, avoiding relevant (solid and wake) blockage effects. The peak value of the solid blockage is $SB_{max} = A_{bmax}/A_t$×100=0.93% for sAR = 4 and α=10°, A_b and A_t being the wing model and the wind tunnel cross-sectional areas, respectively. Besides, we computed an ultra-low wake blockage factor of E_{wb}=1 × 10^{-4} [26]. Finally, there is also a weak influence of the down-wash effect because the wing model is at a finite distance from the wall of the wind tunnel. Previous Particle Image Velocimetry measurements showed a non-dimensional core radius, r_{core}/c, of trailing vortices ranging between 0.07 and 0.12 in the near and intermediate fields at $z/c \leq$30 from the non-deformed NACA0012 wing model for Re=20-40 × 10^3 with sAR=2 [27,28]. The reader must consider that the larger Re, the smaller the core radius of the trailing vortex [28]. Thus, the ratio between $r_{core}/c \simeq$0.1 and the spanwise length, l, represents only a peak value of 5% for the smallest semi-aspect ratio sAR=2. To sum up, a total of 9 wing models were analyzed, including wing aspect ratios ($sAR = l/c$) equal to 1, 2, and 4 and different levels of imposed longitudinal deflection in the wing model with NACA0012 airfoil: non-deformed, intermediate deformation, and large deformation. Fig. 1 depicts a sketch of the employed models and the experimental setup.

The wind tunnel has a servomotor that controls the wing's horizontal orientation, allowing the angle of attack variation. We tested each model for different angles of attack in an automated sweep. We used a precise 6-axis force/torque sensor (ATI FTD-GAMMA, SI-32-2.5) of accuracy $\pm 0.006N$ to acquire the different local force components, being the force $F_{x'}$ located in the longitudinal direction, $F_{y'}$ in the cross direction and F_z in the vertical one. Then, the global lift force component, F_L, has been defined in a coordinate system aligned with wind direction (see Fig. 2) and computed with the following transformation:

$$F_L = F_{x'} \sin(\alpha) + F_{y'} \cos(\alpha). \quad (1)$$

where we have already subtracted the offset of the force signals, see [23] for details about the experimental procedure. Then, the non-dimensional lift force in the global coordinate system is given by

$$C_L = \frac{2F_L}{\rho U_\infty^2 A} \quad (2)$$

where ρ is the air density at a given wind tunnel (temperature) condition and A is the lateral area of the model, $A = l \cdot c$.

As mentioned above, we have used models with two different imposed deformations along the spanwise direction. Fig. 3 reproduces the profiles of both deformations extracted from actual measurements of wing deformations [25] (originally obtained from a NACA0018 profile with sAR = 6 and Re = 230 × 10^3) together with the non-deformed profile. Specifically, we considered the intermediate deformation to be the deformation experienced for an angle of attack of 5° and the large deformation corresponding to 10° [25]. Note that, in the deformed cases, b length corresponds to the projection of the wing on the z axis, and the total curvilinear wing length is slightly greater.

3. Results

3.1. Validation

We manufactured all the NACA0012 wing models with the same material (aluminum), surface ending, and edge rounding. We compared the measurements of non-deformed wings with previous results for validation purposes with a good agreement [21,23]. Fig. 4 displays C_L as a function of the angle of attack for cases of sAR = 1 and sAR = 2 for Re = 80 × 10^3 and Re = 120 × 10^3 as examples of this validation. Note that there is a small difference in the lift coefficients because the Reynolds values from the literature slightly differ from ours. However, the results show an expected performance since the higher the Reynolds number, the higher the lift coefficients.

3.2. Influence of the deformation

As mentioned in the introduction, the scope of this study is to analyze the influence of wing deformation on its aerodynamic performance, particularly on the lift coefficient. Fig. 5 shows the variation of

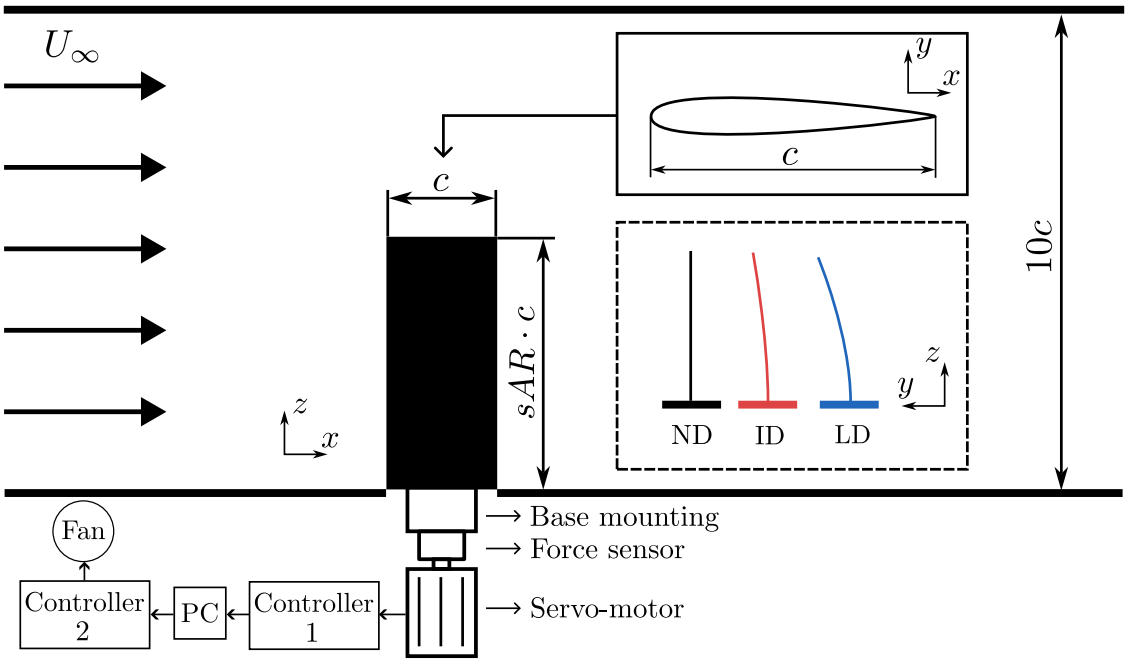

Fig. 1. Experimental setup sketch. The solid inset represents the cross-section of the airfoil. The dashed inset depicts the chord deformation for the three tested configurations: no deformation (ND), intermediate deformation (ID) and large deformation (LD).

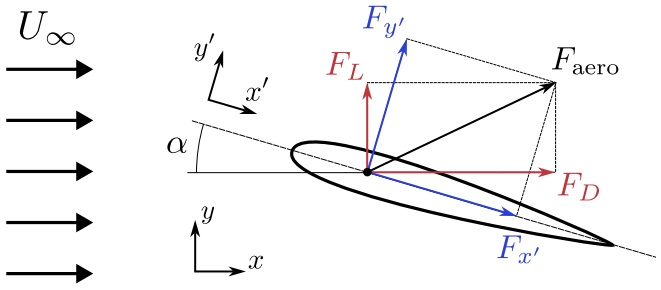

Fig. 2. Airfoil cross-section, representing the orientation of the airfoil for an angle of attack α, and the aerodynamic force components on the local airfoil reference frame $F_{x'}$, $F_{y'}$, and the global wind tunnel reference frame F_L, F_D.

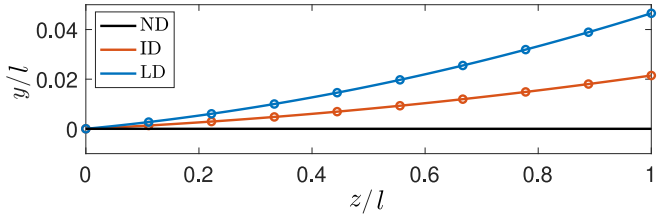

Fig. 3. Non-dimensional deformation levels studied in this work, corresponding to deformations observed from Farnsworth et al. [25].

lift coefficient with the angle of attack, α, for non-deformed models together with deformed ones for several sAR, Re pairs revealing evident differences. Before analyzing these variations, we will focus on some of the singularities inherent in the NACA0012 wing models using non-deformed models. First, it is well known the non-linearity for small Re that can lead even to negative lift coefficients for small positive angles of attack [21,22,29]. The most plausible explanation for the appearance of this zone with negative lift is due to a two-dimensional effect in which there is a pre-alignment of the flow at the leading edge [21]. This non-linear behavior appears in our experiment for $Re = 80 \times 10^3$, especially for $sAR = 2$ and 4. Additionally, Martínez-Aranda et al. [23] showed that there are two different lift slopes (one corresponding to approximately $0 - 3°$ and another one from 3° to the angle of attack corresponding to the stall) using $sAR = 2$ wings. They also report that the change in tendency is more prominent for smaller Reynolds numbers. We observe this change in trend also about 3° for all the $sAR = 2$ cases, from $Re = 80{\times}10^3$ to $Re = 160{\times}10^3$, being more evident in the cases with lower Re. Concerning aspect ratio variations, we have observed that when increasing sAR (see Figs. 5c,f, i), the change in slope is even more evident, whereas, for smaller wings ($sAR = 1$), there is not an apparent change in tendency.

Focusing on the deformed cases, C_L curves are qualitatively similar to non-deformed ones and exhibit the same singularities. The non-linearity also appears for low Re at low angles of attack and is even more noticeable than in non-deformed cases. The trend of the curves also shows a dual slope for high Re and sAR pairs. Nevertheless, while the same qualitative behavior of non-deformed cases is observed, differences appear, and the deformation can slightly modify the lift coefficient for each angle of attack by increasing (in most cases) or decreasing its value.

In general, the influence of the deformation on the lift coefficient becomes more evident for greater sAR and Re and high angles of attack. In particular, for $sAR = 1$ (Figs. 5a,d,g), there is almost no difference between deformed and non-deformed cases. For $sAR = 2$ (Figs. 5b,e,h), differences are subtle for $Re = 80 \times 10^3$, but they grow with Re, and they are evident for $Re = 160 \times 10^3$. For $sAR = 4$ (Figs. 5c,f,i), differences are noticeable for all the analyzed Re values. We can also notice that, in general, C_L differences appear in the second slope region, so for small angles of attack, the effect is almost negligible (except when non-linearity appears), so it starts to grow after a certain angle of attack $\alpha \sim 3°$. Regarding (not shown) drag coefficients, we have observed that wing deformation has a small impact, finding differences below $\Delta C_D < 0.04$ for the tested angles of attack and flow conditions.

To better quantify the effect of the deformation on the lift coefficient, we computed the percentage change on the lift coefficient for a representative $\alpha = 10°$ in which the differences are more evident,

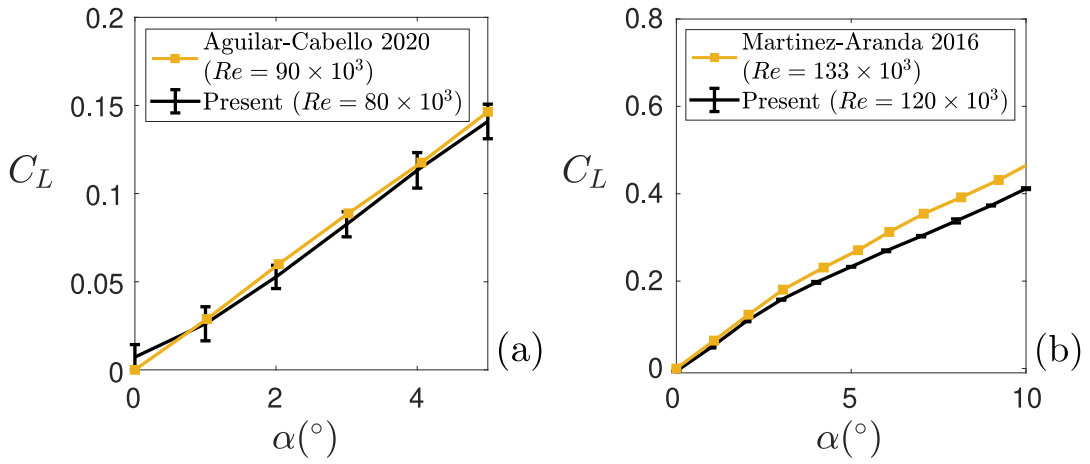

Fig. 4. Lift coefficient, C_L, versus angle of attack, α, for (a) $sAR = 1$ and $Re = 80 \times 10^3$ and (b) $sAR = 2$ and $Re = 120 \times 10^3$. Validation with results from (a) Aguilar-Cabello et al. [21] with $sAR = 1$ and $Re = 90 \times 10^3$ and (b) Martínez-Aranda et al. [23] with $sAR = 2$ and $Re = 133 \times 10^3$.

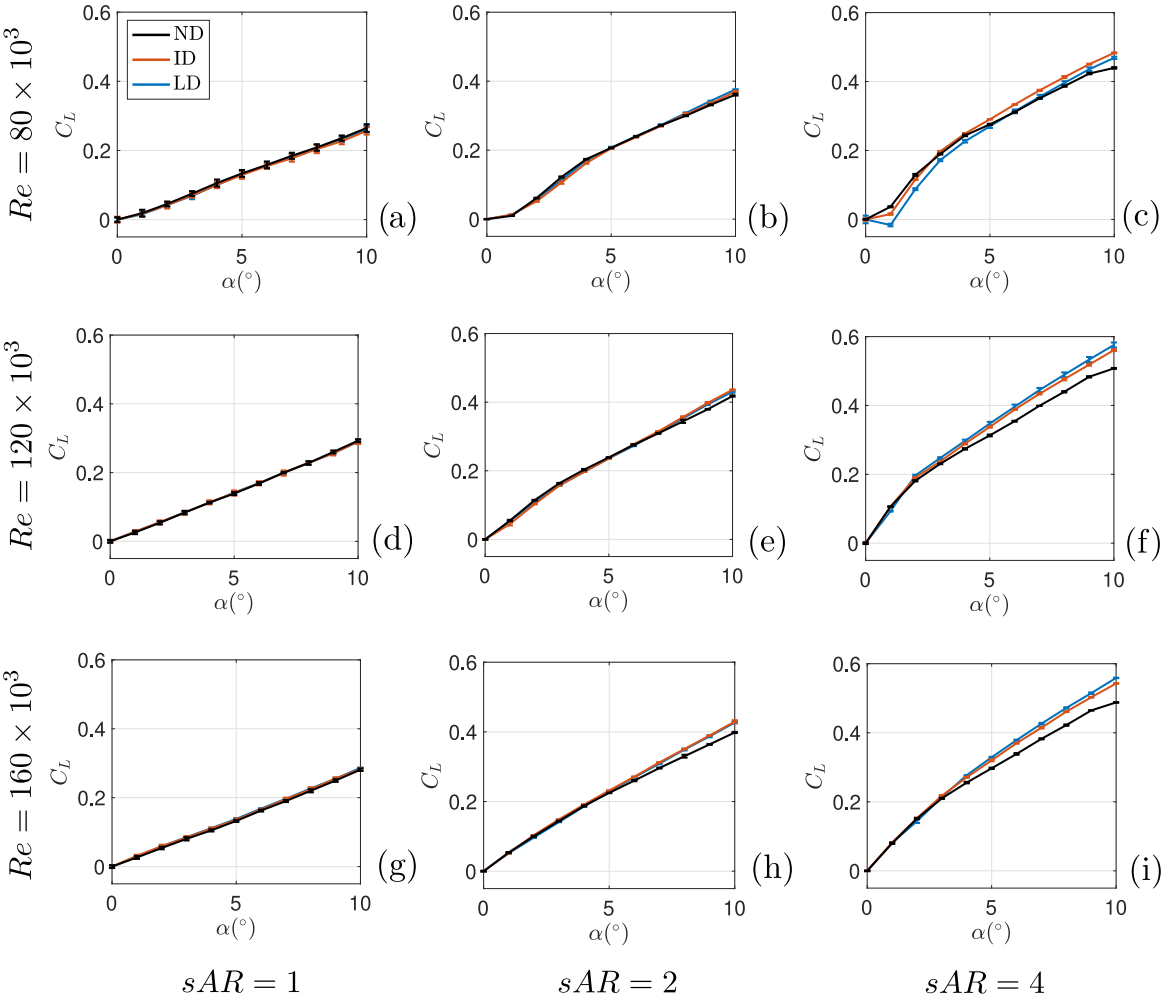

Fig. 5. Evolution of lift coefficient, C_L, versus the angle of attack for several aspect ratios ($sAR = 1, 2, 4$) and flow conditions ($Re = 80, 120, 160 \times 10^3$) for no deformation (black), intermediate deformation (red) and large deformation (blue) wings. (For interpretation of the references to color in this figure legend, the reader is referred to the web version of this article.)

displayed in Table 1. These values show that intermediate and large deformations produce similar lift variations, so the level of the deformation is not proportional to the change in the lift coefficient (this effect is not restricted to the angle of attack $\alpha = 10°$ as is noticeable by insight inspection of the $sAR = 4$ cases, see Figs. 5c,f,i). Note that the intermediate deformation case has a maximum deformation of about 2% of the wingspan, and the large deformation case has a maximum deformation of about 4.5%. However, the maximum lift deviations found for $sAR = 4$ and $Re = 160 \times 10^3$ are 10.5% and 13.4%, respectively, for intermediate and large deformations. In conclusion, a deformation

Table 1
$\Delta C_L = (C_L - C_L^{ND})/C_L^{ND}$ values for intermediate (ID) and large deformation (LD) cases with respect to the non-deformed case (ND), measured at $\alpha = 10°$. Warm and cool colors represent an increase and a decrease of C_L, respectively.

	$sAR = 1$		$sAR = 2$		$sAR = 4$	
	ID	LD	ID	LD	ID	LD
$Re = 80 \times 10^3$	−3.2%	−1.4%	+2.4%	+4.1%	+9.9%	+6.6%
$Re = 120 \times 10^3$	−1.0%	−1.0%	+4.4%	+3.0%	+10.5%	+13.4%
$Re = 160 \times 10^3$	+0.4%	+1.9%	+7.8%	+7.2%	+11.3%	+14.6%

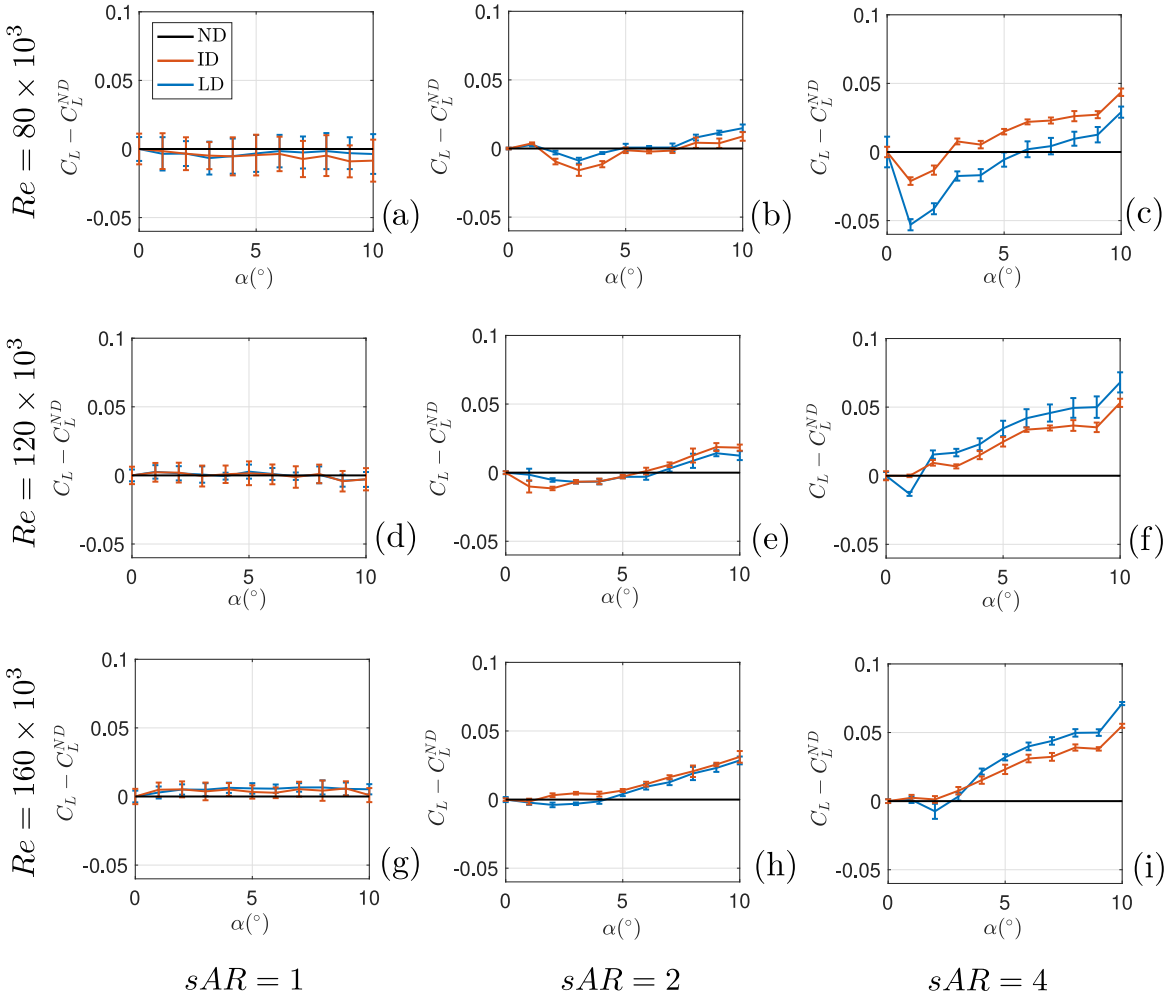

Fig. 6. Difference of the lift coefficient, C_L, for intermediate (red) and large (blue) deformation wings with respect to the non-deformed ones. Several wings ($sAR = 1, 2, 4$) and flow conditions ($Re = 80, 120, 160 \times 10^3$) are shown. (For interpretation of the references to color in this figure legend, the reader is referred to the web version of this article.)

in the wingspan direction, even being very small, significantly impacts the lift coefficient.

Furthermore, the influence of the deformation on C_L is not necessarily homogeneous with the angle of attack. Fig. 6 shows the variation of the C_L depending on α for the cases of study. For $sAR = 1$ (Figs. 6a,d,g), almost no variation is appreciated with deformation, with absolute differences below 0.01 for the range of angle of attack and Reynolds number of the study. Increasing the aspect ratio, that is, for $sAR = 2$ and $sAR = 4$, the increase of C_L grows with the angle of attack for all the cases, showing higher values for high sAR and Re, as displayed in Table 1 for relative differences. Moreover, we observe a particular behavior for low Re cases (Figs. 6b,c,e): we computed negative difference values for low angles of attack, so C_L decreases for deformed cases; then, the difference grows with α, being positive for $\alpha \gtrsim 6°$. The comparison between intermediate and large deformation cases does not provide noteworthy differences. However, differences become more evident for high sAR and Re, showing a slightly higher increase in C_L for the large deformation case.

3.3. Lift slope coefficient $C_{L\alpha}$

The slope of the lift coefficient with the angle of attack, $C_{L\alpha}$, is a key factor in any aerodynamic design. However, its measurement is not straightforward for NACA0012 wing model due to the non-linearity and dual tendencies for certain values of Re, α, and sAR, as indicated. In our study, we have computed a unique slope value for every pair of sAR and Re to get a first approximation of $C_{L\alpha}$, which could be helpful for aerodynamicists. Specifically, we have computed the slope for a linear approximation of the C_L coefficient for $\alpha \in [-7, 7]°$, ensuring that the stall is not considered. This linear approximation is forced to pass through the origin and has associated coefficients of determination of $R^2 > 0.985$ for all the cases. Note that certain designs whose working

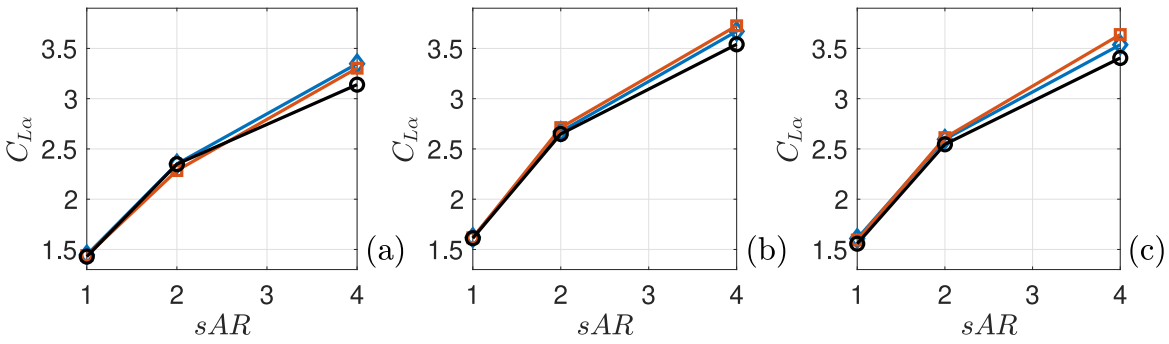

Fig. 7. Lift coefficient slope, $C_{L\alpha}$, evolution for different aspect ratios at (a) $Re = 80 \times 10^3$, (b) $Re = 120 \times 10^3$, (c) $Re = 160 \times 10^3$. Different lines represent non-deformed (black), intermediate deformation (red) and large deformation (blue) cases. (For interpretation of the references to color in this figure legend, the reader is referred to the web version of this article.)

conditions are mainly in the range of NACA0012 singularities may require refinement in the calculations.

The lift slope, $C_{L\alpha}$, increases with Reynolds number and aspect ratio as shown in Fig. 7. This tendency is coherent with the aerodynamic literature. Furthermore, the variation of $C_{L\alpha}$ with Re tends to stabilize after a particular value. An increase of $C_{L\alpha}$ around 10% is observed from $Re = 80 \times 10^3$ to $Re = 120 \times 10^3$, while the values are comparable for $Re = 120 \times 10^3$ and $Re = 160 \times 10^3$.

Regarding the deformation effect on $C_{L\alpha}$, an increase is observed compared to the non-deformed case. This increase is more evident for higher aspect ratio values, reaching a $\sim 10\%$ for $sAR = 4$. Note also that both levels of deformation exhibit similar behavior with comparable increases of $C_{L\alpha}$, even slightly higher for intermediate deformation in some cases. This result is coherent with the ones reported in Section 3.2, where it was stated that the lift variation is not proportional to the level of deformation. Therefore, changes of $C_{L\alpha}$ are not proportional to the deformation either.

3.4. $C_{L\alpha}$ Correlation

Due to the importance of $C_{L\alpha}$, correlations have been proposed in the literature to approximate this parameter for various ranges of Re and AR. Since NACA0012 wing models are relatively thin symmetric profiles, we could try to estimate a first approximation of $C_{L\alpha}$ value using the correlation provided by Gutiérrez-Castillo et al. [20] for a flat plate (which was obtained for the same range of α that our study):

$$C^*_{L\alpha} = \left(\frac{2\pi}{1 + \alpha_1/AR}\right)\left(\frac{\alpha_2}{1 + 10^6/Re}\right)^{1/5}, \tag{3}$$

with $\alpha_1 = 5.21$ and $\alpha_2 = 14.61$ as coefficients of the fitting curve. This empirical correlation is valid for the range of Reynolds numbers Re between $40 - 200 \times 10^3$, and for semi-aspect ratios belonging to $0.5 \leq sAR \leq 4$. Using that expression with the given α_i coefficients, we obtain errors of $\sim 10\%$ on $C_{L\alpha}$. However, we can improve the approximation by setting more suitable α_i values for NACA0012 wing models. First, we computed α_1 and α_2 for our non-deformed cases combined with non-finite length NACA0012 results in the literature. Specifically, we have included experimental results [22,29–31] and numerical results obtained with XFLR5 software, with 2D cases ($sAR = \infty$). Considering all these values, we obtained $\alpha_1 = 6.98$ and $\alpha_2 = 12.13$. In Fig. 8, we show a scatter plot with $C_{L\alpha}$ values compared with those obtained with expression (3), noted as $C^*_{L\alpha}$. We find an excellent agreement with the correlated value for all the data, obtaining a coefficient of determination $R^2 = 0.995$ and a mean quadratic error of $E = 0.01$. Therefore, we can conclude that this correlation, even though it was first proposed for flat plates, permits a good approximation of $C_{L\alpha}$ for NACA0012 wing models with any aspect ratio within its range of validity for Re [20].

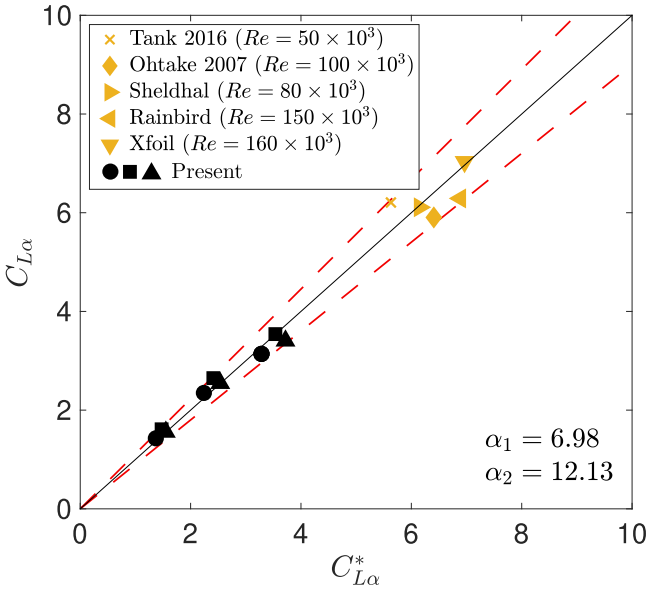

Fig. 8. Scatter plot comparing lift coefficient slope from experimental and numerical results, $C_{L\alpha}$, and from expression (3), $C^*_{L\alpha}$, for non-deformed cases. α_i values represent the coefficients employed to adjust $C^*_{L\alpha}$ fitting curve. Black symbols represent our non-deformed data for $Re = 80 \times 10^3$ (○), $Re = 120 \times 10^3$ (□), and $Re = 160 \times 10^3$ (△). Yellow symbols represent data obtained from the literature and XFRL5 numerical results. Red dashed lines represent the confidence interval of 10%. (For interpretation of the references to color in this figure legend, the reader is referred to the web version of this article.)

To the best of our knowledge, there is no information regarding the influence of the wing deformation in a $C_{L\alpha}$ correlation. When we try to directly approximate $C_{L\alpha}$ for deformed cases using the $C^*_{L\alpha}$ values from the non-deformed NACA0012 α_i coefficients (Fig. 9a), the accuracy is slightly reduced, and the error grows to $E = 0.02$.

The α_1 and α_2 coefficients directly obtained for deformed models, although they provide accurate predictions for $C_{L\alpha}$, have no specific physical meaning. To isolate the effect of the deformation more physically, we fixed $\alpha_2 = 12.13$ obtained for the non-deformed NACA0012 cases since this parameter is related to the Re variations. Then, we calculate α_1, related to the wing aspect ratio, to adjust the correlation for deformed models. In Fig. 9b, we show a scatter plot of $C_{L\alpha}$ vs $C^*_{L\alpha}$ for deformed cases, adjusting $\alpha_1 = 6.60$. We obtain a good accuracy with $E = 0.01$, approximately the same error we obtained mathematically adjusting both α_i values for deformed cases. Therefore, the correlation parameter α_1 can absorb the deformation effect on the lift slope. In conclusion, in terms of the $C_{L\alpha}$, including a deformation in the spanwise direction is equivalent to changing the wing aspect ratio.

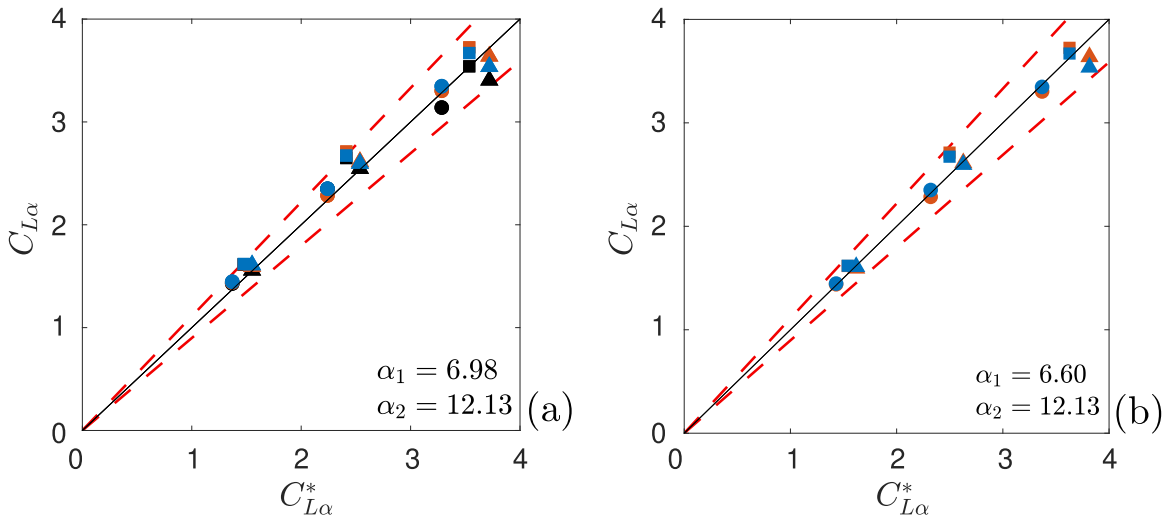

Fig. 9. Scatter plot comparing lift coefficient slope from current experimental results, $C_{L\alpha}$, and from expression (3), $C^*_{L\alpha}$, for (a) non-deformed and deformed cases using α_i values from non-deformed cases (see Fig. 8), and (b) deformed cases readjusting α_1 value. Red dashed lines represent the confidence interval of 10%. (For interpretation of the references to color in this figure legend, the reader is referred to the web version of this article.)

Table 2
Equivalent aspect ratio of a non-deformed wing with the same $C_{L\alpha}$ of the corresponding deformed case. Last row, sAR_C, represents the actual curvilinear length of the deformed wings.

	$sAR = 1$		$sAR = 2$		$sAR = 4$	
	ID	LD	ID	LD	ID	LD
$Re = 80 \times 10^3$	1.07	1.07	2.06	2.16	4.05	4.17
$Re = 120 \times 10^3$	1.13	1.13	2.42	2.36	4.49	4.34
$Re = 160 \times 10^3$	1.04	1.05	2.09	2.07	3.81	3.60
sAR_C	1.0002	1.001	2.0004	2.002	4.0009	4.004

The equivalent length of a non-deformed wing with the same $C_{L\alpha}$ than a deformed case can be estimated with expression (3) using the non-deformed NACA0012 coefficient $\alpha_1 = 6.98$ (and keeping $\alpha_2 = 12.13$ since this parameter was not altered when including the effect of the deformation). Table 2 summarizes the sAR values of equivalent non-deformed wings in terms of $C_{L\alpha}$ for each deformed wing of the study. We observe that the increment of $C_{L\alpha}$ corresponds with the effect of a length increase up to $\sim 20\%$ if non-deformed wings were considered. Note that, as explained in Section 2, the spanwise deformation entails a higher curvilinear wing length, sAR_C, but this value is a much smaller value than the equivalent increment from the deformation effect since the imposed deformations are very small (2% and 4.5% of maximum deformation in the wingspan). The values of sAR_C are also included in the last row of 2 to facilitate the comparison between the actual length increment when imposing the deformation and the effect that would produce on $C_{L\alpha}$ a non-deformed wing with a different sAR. In general, we can conclude that the impact of including a slight deformation in $C_{L\alpha}$ is more pronounced than increasing the size of a straight wing.

4. Conclusion

We have measured the lift coefficients of several NACA0012 rigid models with and without an imposed passive deformation in the wingspan direction, showing how this deflection significantly affects their lift. Specifically, we have studied two deformation levels, around 2% and 4.5% of the wing length, for three different aspect ratios and Reynolds numbers, thus confirming that both deformation levels give a comparable lift coefficient increment. This lift change is not equal at every angle of attack; therefore, it alters the slope of the lift coefficient, $C_{L\alpha}$, an essential parameter in aerodynamic designs. We have deeply analyzed this slope, raising three crucial conclusions. First, a first approximation of $C_{L\alpha}$ for NACA0012 wing models can be obtained using a flat plate correlation when adjusting two parameters (α_1, α_2, which accounts for AR and Re effect, respectively). This result was obtained with our measurements jointly with literature results to expand it to non-finite wings. Second, we include the influence of a wingspan deformation in the correlation by altering only one of its parameters, equivalent to varying the wingspan. Third, a slight deformation has a high impact in $C_{L\alpha}$, producing an increment of $C_{L\alpha}$ stronger than simply changing a non-deformed wing aspect ratio.

In conclusion, our study quantifies the influence of wingspan passive deformations of the lift slope that most modern aerodynamic designs exhibit. This information is helpful to the estimation of aerodynamic characteristics and, specifically, how it affects the lift slope. To our knowledge, no previous correlations could account for the deformation effect. Therefore, this study opens a new line for future investigations of interest for scientific and industrial applications.

CRediT authorship contribution statement

E. Duran: Writing – review & editing, Writing – original draft, Validation, Formal analysis, Data curation. **M. Lorite-Díez:** Writing – review & editing, Methodology, Investigation, Formal analysis. **N. Konovalov-Shishov:** Methodology, Investigation. **P. Gutierrez-Castillo:** Writing – review & editing, Supervision, Project administration, Conceptualization. **C. del Pino:** Writing – review & editing, Supervision, Project administration, Conceptualization.

Declaration of competing interest

The authors declare that they have no known competing financial interests or personal relationships that could have appeared to influence the work reported in this paper.

Data availability

Data will be made available on request.

Acknowledgments

This work was supported by the Spanish Government PID2021-124692OA-I00 and TED2021-131805B from MCIN/ AEI/10.13039/501100011033/. It is also funded by the Universidad de Málaga through the "Ayudas para proyectos dirigidos por jóvenes investigadores"B1-2020_02,"Caracterización de los parámetros aerodinámicos en distancias alas deformadas", the contract CI-21-396 of the project Ayudas para Proyectos Puente "WALICOM: Control Inteligente de estelas de vehículos terrestres". M.L.D also acknowledges the support from FJC2020-043093-I grant by the Spanish MCIN/ AEI/ 10.13039/501100011033/.

References

[1] C.P. Fagley, J. J. Seidel, T.E. McLaughlin, 53rd AIAA Aerospace Sciences Meeting, 2016.
[2] Z.Y. Pang, C.E.S. Cesnik, E.M. Atkins., 55th Structures, Structural Dynamics, and Materials Conference, Vol. 6, 2014, p. 0330.
[3] T. Xia, H. Dong, L. Yang, S. Liu, Z. Jin, AIP Adv. 11 (2023) 597.
[4] F. Afonso, J. Vale, E. Oliveira, F. Lau, A. Suleman, Prog. Aerosp. Sci. 89 (2017) 40–57.
[5] M. Zhong, S. Zheng, G. Wang, J. Hua, R. Gebbink, Chin. J. Aeronaut. 31 (2018) 429–438.
[6] R. Palacios, J. Murua, R. Cook, AIAA J. 48 (2010) 2648–2659.
[7] C. Howcroft, R.G. Cook, D.E. Calderon, L.A. Lambert, M. Castellani, J.E. Cooper, M.H. Lowenberg, S. Neild, AIAA 15th Dynamics Specialists Conference, 2016.
[8] K. Otsuka, Y. Wang, K. Makihara, J. Comput. Nonlinear Dyn. 16 (2021).
[9] R. Albertani, B.S.J. Hubner, P.G. Ifju, Exp. Mech. 47 (2007) 625–635.
[10] Y. Lian, W. Shyy, D. Viieru, B. Zhang, Prog. Aerosp. Sci. 39 (2003) 425–465.
[11] Q. Guo, Z. Wang, J. Wang, Chin. J. Aeronaut. 34 (2021) 133–142.
[12] R. Addo-Akoto, J. Han, J. Han, Phys. Fluids 34 (2022).
[13] C. Martínez-Muriel, G. Arranz, M. Garcia-Villalba, O. Flores, J. Fluid Mech. 964 (2023).
[14] M. Xu, M. Wei, T. Yang, Y.S. Lee, Eur. J. Mech. B/Fluids 55 (2016) 146–156.
[15] S. Sarkar, S. Chajjed, A. Krishnan, Eur. J. Mech. B/Fluids 37 (2013) 72–89.
[16] H. Lee, J. Jang, S. Lee, Eur. J. Mech. B/Fluids 79 (2020) 165–180.
[17] L. Traub, J. Aircr. 50 (2) (2013) 626–634.
[18] W.F. Phillips, D.F. Hunsaker, J. Aircr. 50 (4) (2013) 1226–1233.
[19] L. Traub, Aerospace 11 (2023) 050701.
[20] P. Gutiérrez-Castillo, J. Aguilar-Cabello, S. Alcalde-Morales, L. Parras, C. del Pino, J. Wind Eng. Ind. Aerodyn. 208 (2021) 104459.
[21] J. Aguilar-Cabello, P. Gutiérrez-Castillo, L. Parras, C. del Pino, E. Sanmiguel-Rojas, Phys. Fluids 32 (2020) 055107.
[22] J. Tank, L. Smith, G.R. Spedding, Interface Focus 7 (1) (2017) 20160076.
[23] S. Martínez-Aranda, A. García-González, L. Parras, J. Velázquez-Navarro, C. del Pino, Int. J. Aerosp. Sci. 4 (2016) 1–8.
[24] T. Lee, Y.Y. Su, Exp. Fluids 53 (2012) 1177–1190.
[25] J.A.N. Farnsworth, S. Corbett, J. Seidel, T.E. McLaughlin, 53rd AIAA Aerospace Sciences Meeting, 2015.
[26] L.-S. Shyu, S.-H. Chuang, Trans. Japan Soc. Aeronaut. Space Sci. 51 (171) (2008) 37–42.
[27] C. del Pino, L. Parras, M. Felli, R. Fernandez-Feria, Phys. Fluids 23 (1) (2011) 013602.
[28] J.H. García-Ortiz, A. Domínguez-Vázquez, J. Serrano-Aguilera, L. Parras, C. del Pino, Comput. & Fluids 180 (2019) 176–189.
[29] T. Ohtake, Y. Nakae, T. Motohashi, J. Japan Soc. Aeronaut. Space Sci. 55 (2007) 439–445.
[30] R.E. Sheldahl, P.C. Klimas, Aerodynamics Characteristics of Seven Symmetrical Airfoil Sections Through 180 Degree Angle of Attack for Use in Aerodynamics Analysis of Vertical Axis Wind Turbines, Tech. Rep., Sandia National Labs., Albuquerque, NM (USA), 1981.
[31] J. Rainbird, J. Peiró, J. Graham, J. Wind Eng. Ind. Aerodyn. 145 (2015) 209–218.